HHS Public Access

Author manuscript

Anal Chem. Author manuscript; available in PMC 2023 August 21.

Published in final edited form as:

Anal Chem. 2023 January 17; 95(2): 1047–1056. doi:10.1021/acs.analchem.2c03749.

Unknown Metabolite Identification Using Machine Learning Collision Cross-Section Prediction and Tandem Mass Spectrometry

Carter K. Asef,
School of Chemistry and Biochemistry, Georgia Institute of Technology, Atlanta, Georgia 30332, United States

Markace A. Rainey,
School of Chemistry and Biochemistry, Georgia Institute of Technology, Atlanta, Georgia 30332, United States

Brianna M. Garcia,
Complex Carbohydrate Research Center and Department of Chemistry, University of Georgia, Athens, Georgia 30602, United States

Goncalo J. Gouveia,
Complex Carbohydrate Research Center and Department of Biochemistry, University of Georgia, Athens, Georgia 30602, United States

Amanda O. Shaver,
Complex Carbohydrate Research Center and Department of Genetics, University of Georgia, Athens, Georgia 30602, United States

Franklin E. Leach III,
Complex Carbohydrate Research Center and Department of Environment Health Science, University of Georgia, Athens, Georgia 30602, United States

Alison M. Morse,
Department of Molecular Genetics and Microbiology, University of Florida, Gainesville, Florida 32611, United States

Arthur S. Edison,

Corresponding Author Facundo M. Fernández – *School of Chemistry and Biochemistry and Petit Institute of Bioengineering and Biotechnology, Georgia Institute of Technology, Atlanta, Georgia 30332, United States;* facundo.fernandez@chemistry.gatech.edu.

Author Contributions

C.K.A. performed all LC–MS and IM–MS experiments, B.M.G. provided help with LC–MS experiments and extraction protocols, and M.A.R. and C.K.A. conducted CCS predictions. G.J.G. and A.O.S. grew *C. elegans* samples and maintained colonies. A.M.M. and L.M.M. conducted data processing steps and statistical analysis. F.E.L., A.S.E., and F.M.F. provided overall guidance in experimental design and research strategy. C.K.A. and F.M.F. wrote the manuscript and the rest of the authors edited it. All authors have given approval to the final version of the manuscript.

Supporting Information

The Supporting Information is available free of charge at https://pubs.acs.org/doi/10.1021/acs.analchem.2c03749.
Chromatographic matching curves, data processing steps for LC–MS data, performance metrics for CCS predictions, individual examples of CCS filtering performance, list of internal standards used, details of chromatographic gradients, MS instrument parameters, oPLS-DA parameters, genetic algorithm parameters, and list of failure points observed for each investigated metabolite failing to complete the annotation workflow (PDF).

The authors declare no competing financial interest.

Complex Carbohydrate Research Center, Department of Chemistry, and Department of Biochemistry, University of Georgia, Athens, Georgia 30602, United States

Lauren M. McIntyre,
Department of Molecular Genetics and Microbiology, University of Florida, Gainesville, Florida 32611, United States

Facundo M. Fernández
School of Chemistry and Biochemistry and Petit Institute of Bioengineering and Biotechnology, Georgia Institute of Technology, Atlanta, Georgia 30332, United States

Abstract

Ion mobility (IM) spectrometry provides semiorthogonal data to mass spectrometry (MS), showing promise for identifying unknown metabolites in complex non-targeted metabolomics data sets. While current literature has showcased IM–MS for identifying unknowns under near ideal circumstances, less work has been conducted to evaluate the performance of this approach in metabolomics studies involving highly complex samples with difficult matrices. Here, we present a workflow incorporating *de novo* molecular formula annotation and MS/MS structure elucidation using SIRIUS 4 with experimental IM collision cross-section (CCS) measurements and machine learning CCS predictions to identify differential unknown metabolites in mutant strains of *Caenorhabditis elegans.* For many of those ion features, this workflow enabled the successful filtering of candidate structures generated by *in silico* MS/MS predictions, though in some cases, annotations were challenged by significant hurdles in instrumentation performance and data analysis. While for 37% of differential features we were able to successfully collect both MS/MS and CCS data, fewer than half of these features benefited from a reduction in the number of possible candidate structures using CCS filtering due to poor matching of the machine learning training sets, limited accuracy of experimental and predicted CCS values, and lack of candidate structures resulting from the MS/MS data. When using a CCS error cutoff of ±3%, on average, 28% of candidate structures could be successfully filtered. Herein, we identify and describe the bottlenecks and limitations associated with the identification of unknowns in non-targeted metabolomics using IM–MS to focus and provide insights into areas requiring further improvement.

Graphical Abstract

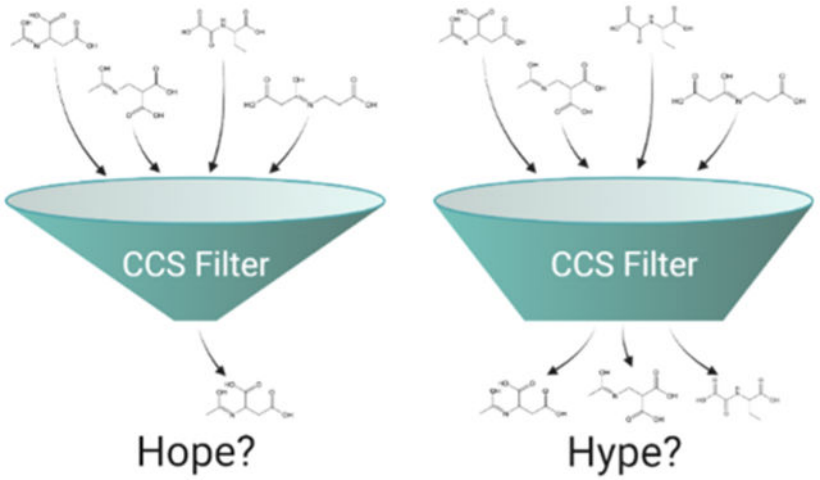

Liquid chromatography mass spectrometry (LC–MS) remains a powerful technique for interrogating perturbations of small molecules in living organisms through non-targeted metabolomics studies. To relate detected ion features to biological processes, annotation of such features must be performed to assign a structure. This is typically accomplished by collecting MS/MS spectra for features of interest and searching against large databases of previously characterized or computationally predicted MS/MS databases such as the human metabolome database,[1] LIPID MAPS structure database,[2] and MassBank.[3] For well-characterized cell lines and organisms, database searches will typically annotate 10% or less of measured features as the coverage of such databases is still incomplete.[4] Annotation of this remaining “metabolic dark matter” is a lengthy process and remains a critical bottleneck in the field of metabolomics.[5]

Limited structural information can be gleaned from the fragment masses of a small molecule’s product ion MS/MS spectrum, though full structural elucidation is not often possible with this information alone. Computed fragmentation trees (e.g., from graph theory) have been proposed as a solution to leverage this limited information, providing likely substructures in the unknown molecules.[6] These trees are visualized as a graph of masses and their related molecular formulas showing the logical progression from precursor to product ion, neutral and radical losses, and subsequent products resulting from multiple fragmentation pathways. CSI:FingerID is an *in silico* machine learning (ML) method that successfully extracts structural motifs (or “molecular fingerprints”) from fragmentation trees, which can then be compared against large databases of molecules without archived MS/MS data.[7] This allows for the molecular fingerprint of an unknown feature to be compared against the millions of entries in molecular structure databases such as PubChem to produce a list of ranked candidate structures. This approach has shown promise in the critical assessment of small molecule identification contests as a part of the SIRIUS 4[8] suite of compound identification tools where it was able to correctly identify 74.8% of features in the top 10 ranked candidates for positive ion mode LC–MS/MS data.[8] Several other computational methods have been proposed that similarly offer a large advantage over manually reviewing MS/MS data, though all generate large lists of candidates that may or may not contain the correct structure in the top ranks.[9]

Ion mobility (IM) spectrometry readily pairs with LC–MS analysis (LC–IM–MS) and offers semiorthogonal information in the form of collision cross-section (CCS) values, a two-dimensional, rotationally averaged representation of molecular size and shape. These CCS values can be derived experimentally from the drift time of an ion feature in the case of drift tube IM (DTIM) or can be calibrated from known DTIM CCS values in the case of traveling wave IM (TWIM).[10] CCS databases have been developed recently along with machine learning (ML) tools that leverage these experimental values to predict the CCS of molecular structures of interest.[11-13] As CCS is an intrinsic trait of a given molecule, it has been touted as a means to further filter candidate structures generated by *in silico* MS/MS analysis software. ML can then be used to computationally predict CCS values of MS/MS candidate structures and filter those by comparison against the measured CCS value.[13] This process is highly dependent on the accuracy of the analytical IM–MS CCS measurement and the ML prediction errors of CCS values, as isomers often vary by less than 2% in CCS.[14] CCS intra-lab variability is commonly reported to be in the 2% range for DTIM–MS measurements of small molecules when using carefully matched IM–MS parameters.[15] These differences call into question the true efficacy of CCS as a means of filtering similar structure candidates.[14] These challenges are further amplified when attempting to compare CCS data acquired by TWIM–MS or other IM–MS techniques against DTIM–MS databases due to the complexities of the calibration procedures involved.[16,17]

To evaluate the capabilities of these tools when applied in a complex, non-targeted metabolomics scenario, our study centered on the LC–MS metabolomics study of *Caenorhabditis elegans* strains with known mutations to central metabolism pathways. Primary LC–MS analysis was conducted on an Orbitrap platform leveraging its high resolution, robust mass accuracy, and iterative data-dependent acquisition (DDA) capabilities to accurately facilitate the elemental formula assignment and provide deep MS/MS coverage. The Orbitrap data set was used to identify differential features of interest to be annotated and generate candidate structures through MS/MS analysis in SIRIUS 4.[8] Following this primary analysis, pooled samples were reanalyzed on a q-IM-TOF instrument to measure CCS values for differential features of interest using LC–TWIM–MS. Candidate structures with ML-predicted CCS values having >3% error against the experimentally measured CCS values were then discarded. CCS predictions proved useful in many cases, but it was also observed that the CCS accuracy currently achievable with commercial IM–MS instruments was sometimes insufficient for unequivocal filtering. These predictions were achieved with high accuracy for many metabolites using machine learning. However, this was not possible for all ion adducts due to limitations in the available training sets. Tandem MS and IM–MS data were successfully collected for 37% of the differential features in the study, with about half of these features benefiting from reduction in candidate structures through IM–MS measurements. Overall, combining IM–MS CCS machine learning predictions with molecular fingerprints obtained from tandem MS fragmentation trees to speed up metabolite annotation was seen as beneficial, with further instrumental IM–MS developments needed for this approach to reach its full potential.

EXPERIMENTAL SECTION

Sample Growth.

Two strains of *C. elegans* (*Caenorhabditis* Genetics Center strains VC1265 and RB2347 with alterations to *pyk*-1 and *idh*-2, respectively) were selected for their mutations to central metabolism pathways and grown in large scale culture plates alongside the PD1074 reference strain samples as previously described.[18,19] Six replicate samples for both test strains were prepared with paired reference samples. Mixed-stage worm populations were harvested, diluted to 200,000 worm aliquots, flash-frozen in liquid nitrogen, and stored at −80 °C. Frozen aliquots were then lyophilized with VirTis BenchTop "K" Series Freeze Dryer (SP Industries, Inc.) and stored at −80 °C until extraction.

Sample Extraction.

Samples were evenly divided across two batches to simultaneously accommodate a maximum of 24 samples including controls through the extraction process. Each mutant strain was represented in both batches to account for extraction batch effects. Lyophilized samples were removed from storage at −80 °C, and three 2.0 mm zirconium oxide beads and 75 μL volume of 0.5 mm glass beads were added to each sample tube. Samples were homogenized in a Qiagen Tissuelyser II for 3 min at 1800 rpm using adapter trays chilled at −80 °C. A sequential extraction was performed starting with the addition of 750 μL LC–MS grade isopropanol (IPA, Fisher Scientific) to each sample. Each sample was lightly vortexed to create a slurry of homogenized samples, which was then transferred to a new 2.0 mL centrifuge tube. This process was repeated a second time, and so, a total volume of 1.5 mL was transferred, leaving behind the homogenizing beads. Samples were vortexed for 1 min and stored overnight (12–15 h) at −20 °C. Samples were centrifuged at 22100G for 5 min, and the supernatants were transferred to new 2.0 mL centrifuge tubes labeled for reverse phase (RP) chromatography. These extracts were dried in a Labconco CentriVap concentrator until completely dry (4–5 h) and stored at −80 °C until LC–MS analysis. The remaining pellet was subjected to a second round of extraction using 1.5 mL of 80:20 LC–MS grade methanol:water (Fisher Scientific). The pellet and methanol:water mixture was shaken at room temperature (23.0 °C) at 1500 rpm for 30 min using a Fisher Scientific Isotemp High Speed Shaker. Samples were again centrifuged at 22100G for 5 min and supernatants were transferred to new 2.0 mL centrifuge tubes labeled for hydrophilic interaction liquid chromatography (HILIC), dried, and stored at −80 °C.

Sample Reconstitution and Pooling.

Dried IPA extracts were reconstituted with 75 μL IPA containing isotopically labeled lipid standards, vortexed for 1 min, centrifuged at 22100G for 5 min, and transferred to 300 μL LC–MS vials for RP LC–MS analysis. Methanol:water extracts followed the same reconstitution steps but were instead reconstituted in 80:20 LC–MS grade methanol:water containing isotopically labeled small molecule standards for HILIC LC–MS analysis. Standards used for each extract are described in Table S1. A total of 5 μL from each PD1074 reference sample in the first batch was taken to create a pooled PD1074 sample. Similarly, 5 μL from each mutant strain sample was taken to create a pooled mutant sample.

Equal volumes from each pool were mixed to create whole batch pool samples. This pooling process was repeated for batch two.

LC–MS Analysis.

Instrument runs began and ended with instrument controls, whole batch pool samples, mutant pool samples, and PD1074 pools. Individual test samples were randomized throughout the middle of the run with three injections of whole batch pool samples interleaved.

IPA samples were LC–MS analyzed using a ThermoFisher Vanquish chromatograph and Accucore C30 150 × 2.1 mm, 2.6 μm column coupled to a ThermoFisher Orbitrap ID-X Tribrid mass spectrometer. Elution was performed using 40:60 water/acetonitrile with 10 mM ammonium acetate (mobile phase A) and 10:90 acetonitrile:isopropyl alcohol with 10 mM ammonium (mobile phase B). Methanol:water extracts were analyzed on the same system using a Water BEH Acquity UPLC BEH Amide column (2.1 × 150 mm, 1.7 μm particle size). Elution was performed using 80:20 water/MeCN with 10 mM ammonium formate and 0.1% formic acid (mobile phase A) and MeCN and 0.1% formic acid (mobile phase B). Batches were run in positive and then negative ion polarity before running subsequent batches. Complete chromatographic settings and mass spectrometer parameters for both chromatographic methods are outlined in Tables S2-4.

Full scan MS1 data for each sample were obtained at a resolution setting of 240,000 full-width half maximum. MS/MS analysis was performed on whole batch pooled samples using three rounds of iterative DDA (ThermoFisher AcquireX) at a resolution of 30,000 FWH using a 0.8 Da isolation window and stepped HCD collision energies of 15, 30, and 45 V.

Whole batch pooled samples were re-analyzed on a Waters Synapt G2-S paired to a Water Acquity I-Class UPLC system using matched chromatography to obtain IM drift times from representative samples. Extensive tuning of IMS parameters was performed to limit fragmentation of small molecule species. Briefly, wave voltages and nitrogen gas pressures within the mobility cell were reduced and a wave velocity gradient was implemented to maintain suitable IM resolution. Instrument parameters are described in Table S4. CCS calibration was accomplished using poly-DL-(alanine) (n = 2–14) (MilliporeSigma). Multiple reference values for poly-DL-(alanine) were evaluated for their ability to yield accurate CCS values for a wide range of small molecule standards.

Data Processing.

Compound Discoverer 3.1 (ThermoFisher) was used to extract spectral features from the Orbitrap ID-X data sets. Processing steps included retention time (RT) alignment, peak picking, feature grouping, peak integration, and gap filling. The first stage of feature annotation was performed through Compound Discoverer 3.1 using mzCloud (ThermoFisher) and in-house mzVault libraries. For analysis of LC–IM–MS data sets acquired on the Waters Synapt G2-S platform, data processing was performed using Progenesis QI 2.4 (Nonlinear Dynamics) to extract features from the raw data and assign CCS values. To match the CCS values of features measured on the Synapt G2-S platform to

features measured on the Orbitrap ID-X platform, the RT of internal standards was used to align the chromatographic scales (Figure S1). Following RT correction of the Synapt G2-S data using a linear calibration curve, a 10 ppm *m/z* tolerance and 0.2 min RT tolerance was used for matching features between platforms manually. In rare cases where multiple features fell within the tolerance window, the Orbitrap ID-X data were manually reviewed to determine the elution order to properly match CCS values.

To control for sample variation, a ranked ANOVA approach was used to determine statistically significant differential features for each mutant strain (see Figure S2 and additional text in Supporting Information). Features were ranked from most intense to least intense within each sample and binned across 1,000 bins. ANOVA was then performed on the bin number between the mutant and control samples using the Galaxy web platform.[20] Bin numbers for features with $p < 0.05$ were used to construct orthogonalized partial least-squares discriminant analysis (oPLS-DA) models within PLS_toolbox 8.9.1 (Eigenvector Research, Inc.) with the parameters described in Tables S5-S6. Features with top VIP scores were reviewed for proper chromatographic integration and further interrogated for structural identification. At least 10 features from each polarity and chromatography mode were investigated for both mutants.

Prediction of Candidate Structures and CCS Values.

MS/MS data were exported from Compound Discoverer 3.1 in.mgf file format and imported into SIRIUS 4.9.3[8] to predict the most likely elemental formula and adduct species for each feature based on *m/z*, isotope intensity, and fragmentation pattern. CSI:FingerID[7] was used within SIRIUS 4.9.3[8] to generate candidate structures for each feature. Resulting candidate structures were written to.csv files containing the corresponding InChI codes.

To predict CCS values, two data sets were created using the Unified CCS Compendium,[11] one containing all entries for $[M + H]^+$ adduct species and another set for all $[M - H]^-$ entries ($n = 644$ and 582, respectively). These data sets were then randomly split 75% into training sets and 25% into test sets, which were used to construct a support vector regression (SVR)-based ML model using CCSP 2.0,[21] as illustrated in Figure 1. Using the optimized SVR models, CCS values for any given candidate structure could be predicted for $[M + H]^+$ and $[M - H]^-$ species from their neutral InChI code. The predicted CCS value for each candidate structure was compared against the experimental value obtained from LC–IM–MS data. The accuracy of the predictions was evaluated using the following eq 1

$$\frac{\mathrm{CCS}_{\mathrm{experimental}} - \mathrm{CCS}_{\mathrm{predicted}}}{\mathrm{CCS}_{\mathrm{predicted}}} \times 100\,\% \quad (1)$$

Structures with >3% error were discarded.

RESULTS AND DISCUSSION

Challenges Integrating IM–MS in an LC–MS *C. elegans* Metabolomics Pipeline.

To evaluate the utility of IM–MS for unknown feature annotation under practical conditions, we developed and tested an experimental workflow that included several innovative steps

(Figure 2). Two *C. elegans* strains with mutations to central metabolism pathways (RB2347 and VC1265) were grown alongside reference strain samples to serve as a representative case/control case study for non-targeted metabolomic analysis. The samples consisted of a complex matrix derived from the nematodes, growth media, and buffers used. Six samples of the RB2347 and VC1265 mutant strains were prepared together with a growth-matched reference strain sample for each. These samples were sequentially extracted to produce polar and nonpolar fractions. LC–MS analysis of each extract was first performed on an Orbitrap ID-X (ThermoFisher) in both ion polarities. RP chromatography was used for nonpolar extracts and HILIC for polar extracts. This procedure yielded four data sets (RP/HILIC, positive/negative, several Gb each). Orbitrap LC–MS results showed high mass accuracy (<3 ppm), whereas iterative DDA AcquireX runs on pooled samples allowed for deep MS/MS coverage. From the collected data sets, pre-selection of statistically significant differential features between controls and mutants was performed using a ranked ANOVA approach. Once feature selection via ANOVA was completed, it was followed by oPLS-DA modeling. From these oPLS-DA models, a short list of features with the highest VIP scores was created. These features were used as test cases for attempting metabolite annotation using the workflow in Figure 2. A total of 95 features were investigated for structural annotation, 56 of which had MS/MS data collected by iterative DDA. The remaining features were not selected after three rounds of iterative DDA and were not pursued further. Between 2 and 784 candidate structures were generated for each one of these features in SIRIUS 4[8] using CSI:FingerID,[7] showing the wide diversity of structures possible from a given MS/MS spectrum when only a few informative fragment ions are present. The CCS for each candidate structure was predicted using the ML CCSP 2.0 algorithm. CCS prediction was not possible for all features as only $[M + H]^+$, $[M + Na]^+$, and $[M - H]^-$ adduct species had sufficient training data available in the Unified CCS Compendium[11] to build accurate ML models. A total of 66% of the features were detected as one of these adducts, meaning that CCS prediction was possible for approximately two-thirds of the features investigated. Creation of training sets for other types of adducts is an area in need of further research, as shown in detail in Table S7.

Pooled *C. elegans* samples were analyzed on the Synapt G2-S platform to collect TWIM-MS data and provide experimentally measured CCS values for features of interest. Matched chromatography was used, though RT correction using internal standards was required. Features detected in the Orbitrap ID-X platform could then be aligned to those measured on the Synapt G2-S by matching them with 10 ppm and 0.2 min. RT error after correction. A total of 55 out of the 95 differential features were matched using these criteria and could be assigned experimental CCS values. The lowest observed success rate was for lipid species in the RP data set. Some of these were only observed as dimeric ions (e.g., $[2M + H]^+$) on the Orbitrap ID-X but not detected on the Synapt G2-S. It is possible that these dimeric ions either do not form as readily in the Synapt instrument ion source or that these species do not survive more complex ion optics, which include the higher-pressure IM cell, without fragmenting. Features from the HILIC Orbitrap data set were also sometimes missing in the Synapt data set, likely due to unwanted ion activation in the mobility stage or differences in ion transmission between platforms.

Fragmentation products observed for labile metabolites during LC–TWIM–MS method development with standard metabolites included amino acid deamination, decarboxylation of organic acids, and fragmentation of compounds such as hippuric acid. Extensive tuning of the IM parameters was performed to minimize unwanted fragmentation of small molecules occurring during ion transport from the higher vacuum quadrupole region into the higher-pressure mobility cell of the instrument. The final IM–MS parameters chosen to minimize fragmentation are given in Table S4. Another reason that could lead to the lack of matched features between the Orbitrap and Synapt systems is related to differences in their mass resolution. It is possible that spectral overlaps in the lower resolution Synapt platform resulted in the mass errors that caused features to fall outside the 10 ppm window.

Candidate structures for the investigated differential features could be filtered once these were assigned experimental CCS values from TWIM–MS data, candidate structures from Orbitrap MS/MS data, and ML-predicted CCS values. The differences observed between ML-predicted *vs* experimental CCS values are a complex convolution of several factors that include (1) the experimental TWIM–MS CCS measurement and calibration errors and (2) the SVR model errors inherent to ML predictions. Regarding the latter, multiple attempts to accurately predict the uncertainty of SVR models via bootstrap approaches[22-24] have been done, but none have yet been implemented in the context of CCS prediction algorithms. The considerable number of molecular descriptor inputs and the lack of comprehensive training data complicate the generation of point-wise confidence intervals for each metabolite of interest. Consequently, CCS prediction algorithms typically rely on summary statistics such as the root mean square error (RMSE) and the median relative error to set blanket exclusion thresholds. Most CCS prediction algorithms in the literature suggest a 3% threshold for matching the experimentally measured CCS and the predicted CCS values of their test sets.[25-27] Though more restrictive (1%) and more permissive[13] (4%) thresholds have also been investigated, a 3% filtering threshold was adopted here based on the calibration errors observed in our experiments and to allow for comparison between our results and those previously published.

Machine Learning CCS Predictions.

CCSP 2.0, our in-house ML algorithm for CCS prediction, encodes the molecular structure through neutral InChI strings and uses molecular descriptors for such structures to generate SVR models that accurately predict CCS for unknown ions (Figure 1). This ML tool was created in a Jupyter notebook with freely available open-source Python packages for maximum accessibility and to enable the user to modify the code as needed. Prior to applying CCSP 2.0 to the *C. elegans* IM–MS data set, its prediction accuracy was estimated through an external validation procedure. All models were created for specific ionic species, such as $[M + H]^+$, $[M - H]^-$, and so forth. The CCS prediction error was 1.14% for $[M - H]^-$ ions and 1.56% for $[M + H]^+$ ions. These errors corresponded to RMSE values of 4.268 and 5.694 $Å^2$, respectively, which were comparable to or better than other published CCS prediction methods.[12,13] Further CCS prediction cross-validation results are provided in Figure S3, showing an excellent correlation between measured and predicted CCS values. This level of prediction accuracy, together with the flexible CCSP 2.0 code environment, allows other research teams to adapt the training set to their specific applications and to

make use of hybrid calibration strategies combining experimental and predicted CCS values, as discussed in the next section and in Figure 3.

Optimizing TWIM Calibration Accuracy for Diverse Data sets.

Minimizing CCS calibration errors is a critical component in obtaining the most accurate CCS values for filtering structures generated in SIRIUS 4. TWIM-MS CCS measurements ($^{TW}CCS_{N2}$[28]) require calibration of drift times with a series of compounds with known CCS values, typically measured by DTIM–MS ($^{DT}CCS_{N2}$). Poly-DL-(alanine) oligomers are commonly used as a calibrant mixture because they exhibit relatively little chemical class bias. This makes this calibrant well suited for non-targeted IM–MS analysis.[29-32] The source of $^{DT}CCS_{N2}$ reference values plays a large role in the quality of the results produced by TWIM–MS following drift time calibration. Ideally, calibration should be performed using data from the database source that will ultimately be used for comparisons. For example, TWIM–MS drift times calibrated using Unified CCS Compendium[11] $^{DT}CCS_{N2}$ values will have the highest agreement with other CCS data from this source if compared to data from alternative sources such as AllCCS[13] and CCSbase.[12] However, the CCS reference database of choice often may not include complete data for the desired calibrant series. In our case, the Unified CCS Compendium[11] only reports CCS values for poly(alanine) down to the $n = 4$ oligomer ($[M + H]^+ = m/z$ 303.1668) though the range of differential metabolites investigated spanned m/z values between 70 and 1050. While power-law calibrations can be used to extrapolate CCS values outside of the calibrated range, it is possible that including additional calibration points to cover the expected m/z range may further improve results. To achieve greater CCS calibration coverage, we tested four different calibration methods. The basic method only used the poly(alanine) CCS values from the Unified CCS Compendium.[11] A second method supplemented the Unified CCS Compendium poly(alanine) data with Compendium values from tryptophan and dimethylglycine. A third calibration method used the full poly(alanine) CCS reference data from Hines et al.,[30] which includes the $n = 2–3$ oligomers. The fourth and last calibration approach used ML-predicted CCS values for the $n = 2–3$ oligomers obtained when using Unified CCS Compendium[11] data for the training set.

The accuracy of these four calibration methods was compared by measuring CCS values of 14 chemical standards covering the m/z 104–241 range in positive ion polarity. A single IM–MS data set was acquired and then calibrated using each of the four calibration methods. Calculated CCS values were then compared against those reported in the Unified CCS Compendium. Resulting errors are shown in Figure 3. On average, the least agreement (% average absolute error = 1.84) was observed when calibrating with data from Hines et al. and comparing against the Unified CCS Compendium (Figure 3c). These differences likely arise from benchmarking data calibrated with reference values from one laboratory against the values from another laboratory. It may also arise from the inherently different TWIM and DTIM gas-phase separation mechanisms. CCS data calibrated using only CCS Compendium poly(alanine) values yielded the lowest average absolute error (1.23%, Figure 3a). Calibration with additional standards (Figure 3d) produced an absolute error of 1.68% on average, and calibration supplemented with ML-predicted points performed similarly to the approach involving additional standards, with an average absolute error of 1.62%

(Figure 3b). The latter results illustrate the possibility of enhancing TWIM calibrations with ML-derived values in cases where the reference database is incomplete. Figure 3e shows the results for each of the individual standard compounds tested. Based on these results, the method depicted in Figure 3a was selected moving forward as it yielded absolute errors ranging from 0.02 to 2.98%. Based on these calibration errors, the chosen CCS threshold of 3% for comparing predicted and experimental CCS values was in line with literature results.

Distribution of ML CCS Prediction Errors for SIRIUS 4-Derived Structures.

The errors of the experimentally measured *versus* ML predicted CCS values for each candidate structure generated in SIRIUS 4 were calculated for all 19 differential features investigated. Histograms of these measured *versus* predicted CCS error distributions are shown in Figure 4. The overall success of the annotation workflow CCS filtering step can be evaluated from the results shown in Figure 4a. A total of 1580 (45%) candidate structures were filtered out from the original 3495 structures proposed by SIRIUS 4. Interestingly, an overall shift toward negative errors was observed in the histogram. This effect can likely be attributed to the choice of polyalanine for converting TWIM drift times to CCS values (Figure 3e). Bias in the calibration may be introduced by the nuanced interactions of the chosen calibrants with the transient electric fields present in the TWIM drift cell. These interactions change based on the chemical class in ways not accounted for in typical power-law drift time calibrations, such as the one used here.[16] As a result, chemical class differences between the calibrant and analyte manifest as CCS biases in the same direction, positive or negative.[17] While poly(alanine) serves as a general calibrant offering reasonably good structural similarity for a variety of compounds,[29-32] other calibrants could likely exhibit better calibrant–analyte structural similarity. This is important for non-targeted metabolomics studies dealing with a variety of chemical classes, such as those involved in central metabolism mutant *C. elegans* strains. However, chemical class matching of the calibrants to the unknowns is only possible with a priori knowledge of the chemical class of the investigated features. Moreover, current experimental CCS databases often lack sufficient representation from compounds of a certain class of interest, such as adduct ions that could match the ionic species detected.

Error histograms for individual features displayed similar Gaussian-like distributions due to the high similarity of the structures generated from *in silico* analysis of a given MS/MS spectrum. The overall success of CCS filtering was 45%, highlighting the usefulness of the proposed annotation workflow, but it must be borne in mind that the success varied on a feature-by-feature basis. Many candidate structures fell within ±3% of the center of each error distribution, and thus, the percent of features filtered by CCS was dependent on how far the center of such error distribution was shifted from the experimental CCS value. A successful case is shown in Figure 4b where the distribution was centered at roughly −4% error. In this case, the correct structural annotation (*N*-acetyl aspartate) fell on the right shoulder of the distribution, just within the ±3% CCS cutoff. The identity of the correct compound was confirmed with a pure standard and through searches in mzCloud during data processing. *N*-acetyl aspartate represents an almost ideal case where CCS can filter >50% of candidate structures while retaining the correct annotation. Out of the 57 candidate structures within the ±3% CCS cutoff (Figure 4b), *N*-acetyl aspartate was the #1 ranked

SIRIUS 4 candidate. This example, however, is not typical. A less successful scenario is shown in Figure 4c for a yet-unidentified feature at *m/z* 175.0713 and RT 8.02 min, where only 19% of candidate structures fell outside the ±3% CCS cutoff. Figure 4d depicts a case of an unknown with a CCS error distribution shifted toward positive values. In this case, 33% of candidate structures were filtered. The MS/MS and CCS data on the remaining 45 structures were insufficient to make a conclusive annotation. These results highlight the importance of reducing the CCS cutoff value by improving overall CCS measurement accuracy.

Results in Figure 4e indicated a general trend observed in the data set for lipid species. These were especially challenging to annotate due to the multitude of possible isomeric structures of similar molecular size and shape. *In silico* prediction of such structures from MS/MS spectra yields fewer structures than for other classes of compounds, but these all have very similar predicted CCS values. Effectively, this results in a narrower CCS error distribution that is more difficult to filter by TWIM-MS measurements. As expected, this effect was more commonly observed for features in the RP data sets as the extraction step used resulted in lipid-rich systems.

Structural Annotation of Differential Features in *C. elegans* Mutants.

A total of 95 features were identified as differential between the mutant and control strains and further investigated with the proposed workflow. Matched MS/MS and CCS data were successfully collected for 34 of these features. Of these 34, only 19 could be processed through the entire workflow. The effectiveness of CCS filtering for each of these 19 features is shown in Figure 5. Both the number of candidate structures generated and the percent of structures filtered by CCS varied substantially on a case-to-case basis. An average of 183.9 candidate structures were generated for each feature with a mean reduction of 28% of structures on an individual basis using CCS filtering. The average percent of features filtered individually was considerably lower than the overall filtering rate of 45%, as features with more candidate structures tended to have more structures filtered by CCS. Notably, six features had no reduction in candidate structures, meaning that all structures had predicted CCS values within 3% of the measured CCS. For a differential feature at *m/z* 738 and RT 3.1 min in the RP data set, only two of the 233 candidate structures could be filtered. This shows that while many structures may be possible for a given formula, MS/MS data will often constrain the possibilities to those of highly similar molecular size and shape, and therefore, CCS values. For the 15 features which could not be processed through the full annotation workflow, several unique failure points were identified. As previously mentioned, sufficient training data were not available in many cases to construct accurate ML models for the measured type of ion adduct. Other points of failure include (1) no candidate structures from MS/MS data produced by SIRIUS 4, (2) TWIM–MS ion rollover identified as an abnormally small CCS value due to the ions not clearing the mobility cell during a single scan, and (3) incorrect processing of TWIM–MS drift time data by Progenesis software yielding incorrect drift times. A full description of identified challenges for each of the 15 non-identified features is given in Table S7. Though ion rollover and incorrect arrival time assignment could be rectified through follow-up experiments and manual data

processing, it is important to note the challenges in designing an automated workflow that would work universally well on every feature without exception.

Certain assignments were confirmed for three of the 19 successfully investigated features using pure analytical standards by matching RT and drift time from the Synapt G2-S and matching MS/MS spectra from the Orbitrap ID-X. Two of these features were also identified first within mzCloud: *N*-acetyl aspartate and guanine. While these compounds only marginally benefited from CCS candidate structure filtering, CCS still helped as an effective reassurance of the annotation (Figure S4). The MS/MS spectra from *N*-acetyl aspartate generated 376 candidate structures, 85% of which were filtered by CCS. Guanine produced 365 candidate structures, 54% of which were filtered by CCS. The measured CCS values for both features were within 3% of the predicted CCS for the correct structure.

Perhaps the most useful application of the proposed workflow was for the feature at *m/z* 175 and RT 8.3 where only two candidate structures were generated. One of these two structures could be discarded by CCS, leaving only the possibility for allantoic acid, which was later confirmed by *m/z*, RT, and MS/MS matching to a pure standard.

CONCLUSIONS

In this article, we have explored the utility of augmenting non-targeted metabolomics workflows with an ion mobility candidate structure-filtering step to establish the performance of this approach under “real world” conditions involving complex samples. The results indicated that the number of filtered structures was highly variable and limited mainly by the accuracy of CCS measurements and ML predictions achievable with current instrumentation and calibration approaches. With the current CCS cutoff of 3% typically used in the literature, filtering efficacy depended on chemical class and the amount of information that could be gleaned from MS/MS fragment ions. On average, a mean reduction of 28% of structures on an individual basis was observed. These results demonstrate both the promise for applying IM–MS to aid in metabolite identification efforts, but also the need to improve current IM–MS instrumentation to improve accuracy.

An important limitation of our study was that focus was placed only on those discriminating features for which we were able to collect informative MS/MS information. For species without fragmentation information, the number of structure candidates is even higher and therefore annotation becomes more challenging. In these cases, CCS filtering can be leveraged to remove some of the unlikely structures, but full annotation would require complementary approaches such as retention time matching with predicted retention time values or NMR spectroscopy on isolated fractions.

As higher resolution and higher accuracy IM–MS instrumentation is developed, and CCS prediction ML models for additional ionic species become available, we expect that the utility of CCS candidate filtering for metabolite identification will also improve. While many recent advancements have resulted in IM–MS platforms with considerably higher resolution, the work presented here highlights the need for improvements in CCS accuracy, not only resolving power. A greater agreement in measured CCS between platforms

is also highly desirable, requiring improvements in calibration approaches and platform interoperability. New IM–MS platforms, such as trapped IM, cyclic IM, and structures for lossless ion manipulations (SLIM) IM, offer much improved separation capabilities compared to the more standard TWIM–MS platform tested here, but the variance between DTIM CCS values and those platforms is still >1% in most cases. Our results highlight that the current level of accuracy of CCS values is still insufficient for reaching the full potential of IM–MS-based metabolite annotation efforts. Improvements in ML prediction of CCS values through better training sets will also likely reduce one of the main sources of variance in the CCS filtering approach..

Supplementary Material

Refer to Web version on PubMed Central for supplementary material.

ACKNOWLEDGMENTS

Research reported in this manuscript was supported by the National Institutes of Health award number 1U2CES030167-01 (ASE contact PI) and by grant 1R01CA218664-01 to F.M.F. We thank Kenneth M. Merz Jr. and his team for insightful discussions. Elements of Figures 1,2, and S2 were created with BioRender.com.

REFERENCES

(1). Wishart DS; Guo A; Oler E; Wang F; Anjum A; Peters H; Dizon R; Sayeeda Z; Tian S; Lee BL; Berjanskii M; Mah R; Yamamoto M; Jovel J; Torres-Calzada C; Hiebert-Giesbrecht M; Lui VW; Varshavi D; Varshavi D; Allen D; Arndt D; Khetarpal N; Sivakumaran A; Harford K; Sanford S; Yee K; Cao X; Budinski Z; Liigand J; Zhang L; Zheng J; Mandal R; Karu N; Dambrova M; Schiöth HB; Greiner R; Gautam V Nucleic Acids Res. 2021, 50, D622–D631.

(2). Sud M; Fahy E; Cotter D; Brown A; Dennis EA; Glass CK; Merrill AH; Murphy RC; Raetz CRH; Russell DW; Subramaniam S Nucleic Acids Res. 2007, 35, D527–D532. [PubMed: 17098933]

(3). Horai H; Arita M; Kanaya S; Nihei Y; Ikeda T; Suwa K; Ojima Y; Tanaka K; Tanaka S; Aoshima K; Oda Y; Kakazu Y; Kusano M; Tohge T; Matsuda F; Sawada Y; Hirai MY; Nakanishi H; Ikeda K; Akimoto N; Maoka T; Takahashi H; Ara T; Sakurai N; Suzuki H; Shibata D; Neumann S; Iida T; Tanaka K; Funatsu K; Matsuura F; Soga T; Taguchi R; Saito K; Nishioka TJ Mass Spectrom. 2010, 45, 703–714.

(4). Bowen BP; Northen TR J. Am. Soc. Mass Spectrom 2010, 21, 1471–1476. [PubMed: 20452782]

(5). da Silva RR; Dorrestein PC; Quinn RA Proc. Natl. Acad. Sci. U.S.A 2015, 112, 12549–12550. [PubMed: 26430243]

(6). Vaniya A; Fiehn O Trends Anal. Chem 2015, 69, 52–61.

(7). Dührkop K; Shen H; Meusel M; Rousu J; Böcker S Proc. Natl. Acad. Sci. U.S.A 2015, 112, 12580–12585. [PubMed: 26392543]

(8). Dührkop K; Fleischauer M; Ludwig M; Aksenov AA; Melnik AV; Meusel M; Dorrestein PC; Rousu J; Böcker S Nat. Methods 2019, 16, 299–302. [PubMed: 30886413]

(9). Blaženović I; Kind T; Ji J; Fiehn O Metabolites 2018, 8, 31. [PubMed: 29748461]

(10). Paglia G; Astarita G Nat. Protoc 2017, 12, 797–813. [PubMed: 28301461]

(11). Picache JA; Rose BS; Balinski A; Leaptrot KL; Sherrod SD; May JC; McLean JA Chem. Sci 2019, 10, 983–993. [PubMed: 30774892]

(12). Ross DH; Cho JH; Xu L Anal. Chem 2020, 92, 4548–4557. [PubMed: 32096630]

(13). Zhou Z; Luo M; Chen X; Yin Y; Xiong X; Wang R; Zhu Z-J Nat. Commun 2020, 11, 4334. [PubMed: 32859911]

(14). Dodds JN; May JC; McLean JA Anal. Chem 2017, 89, 952–959. [PubMed: 28029037]

(15). Paglia G; Williams JP; Menikarachchi L; Thompson JW; Tyldesley-Worster R; Halldórsson S; Rolfsson O; Moseley A; Grant D; Langridge J; Palsson BO; Astarita G Anal. Chem 2014, 86, 3985–3993. [PubMed: 24640936]

(16). Richardson K; Langridge D; Dixit SM; Ruotolo BT Anal. Chem 2021, 93, 3542–3550. [PubMed: 33555172]

(17). Hines KM; May JC; McLean JA; Xu L Anal. Chem 2016, 88, 7329–7336. [PubMed: 27321977]

(18). Shaver AO; Gouveia GJ; Kirby PS; Andersen EC; Edison ASJ Visualized Exp. 2021, 171, No. e61453.

(19). Shaver AO; Garcia BM; Gouveia GJ; Morse AM; Liu Z; Asef CK; Borges RM; Leach FE; Andersen EC; Amster IJ; Fernández FM; Edison AS; McIntyre LMAn Anchored Experimental Design and Meta-Analysis Approach to Address Batch Effects in Large-Scale Metabolomics. March 27. 2022, bioRxiv, p 2022.03.25.485859.

(20). Afgan E; Baker D; Batut B; van den Beek M; Bouvier D; Čech M; Chilton J; Clements D; Coraor N; Grüning BA; Guerler A; Hillman-Jackson J; Hiltemann S; Jalili V; Rasche H; Soranzo N; Goecks J; Taylor J; Nekrutenko A; Blankenberg D Nucleic Acids Res. 2018, 46, W537–W544. [PubMed: 29790989]

(21). Rainey MA; Watson CA; Asef CK; Foster MR; Baker ES; Fernández FM Anal. Chem 2022, 94 (50), 17456–17466. [PubMed: 36473057]

(22). De Brabanter K; De Brabanter J; Suykens JAK; De Moor B IEEE Trans. Neural Network. 2011, 22, 110–120.

(23). Harrington P de B J. Chemom 2017, 31, No. e2867.

(24). Lins ID; Droguett EL; Moura M das C; Zio E; Jacinto CM Reliab. Eng. Syst. Saf 2015, 137, 120–128.

(25). Zhou Z; Shen X; Tu J; Zhu Z-J Anal. Chem 2016, 88, 11084–11091. [PubMed: 27768289]

(26). Zhou Z; Tu J; Xiong X; Shen X; Zhu Z-J Anal. Chem 2017, 89, 9559–9566. [PubMed: 28764323]

(27). Plante P-L; Francovic-Fontaine É; May JC; McLean JA; Baker ES; Laviolette F; Marchand M; Corbeil J Anal. Chem 2019, 91, 5191–5199. [PubMed: 30932474]

(28). Gabelica V; Shvartsburg AA; Afonso C; Barran P; Benesch JLP; Bleiholder C; Bowers MT; Bilbao A; Bush MF; Campbell JL; Campuzano IDG; Causon T; Clowers BH; Creaser CS; De Pauw E; Far J; Fernandez-Lima F; Fjeldsted JC; Giles K; Groessl M; Hogan CJ; Hann S; Kim HI; Kurulugama RT; May JC; McLean JA; Pagel K; Richardson K; Ridgeway ME; Rosu F; Sobott F; Thalassinos K; Valentine SJ; Wyttenbach T Mass Spectrom. Rev 2019, 38, 291–320. [PubMed: 30707468]

(29). Forsythe JG; Petrov AS; Walker CA; Allen SJ; Pellissier JS; Bush MF; Hud NV; Fernández FM Analyst 2015, 140, 6853–6861. [PubMed: 26148962]

(30). Hines KM; Ross DH; Davidson KL; Bush MF; Xu L Anal. Chem 2017, 89, 9023–9030. [PubMed: 28764324]

(31). Li A; Conant CR; Zheng X; Bloodsworth KJ; Orton DJ; Garimella SVB; Attah IK; Nagy G; Smith RD; Ibrahim YM Anal. Chem 2020, 92, 14976–14982. [PubMed: 33136380]

(32). Ridenour WB; Kliman M; McLean JA; Caprioli RM Anal. Chem 2010, 82, 1881–1889. [PubMed: 20146447]

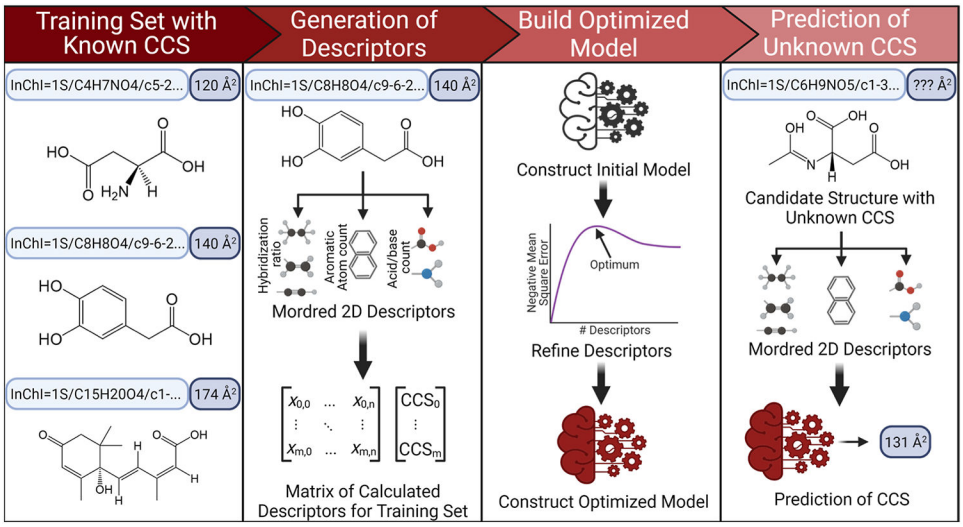

Figure 1.

CCSP 2.0 is an SVR-based machine learning algorithm for predicting CCS values from 2D structures represented by InChI strings. Two-dimensional structural data are first used to calculate up to 1613 quantifiable descriptors for each string in the training set through the Python Mordred package, generating a matrix of descriptors matching the matrix of experimental CCS values. Descriptors not applicable to molecules in the training set are culled and an initial SVR model is constructed. Optimization of the model is performed by limiting the number of descriptors used to those with the highest weights and then identifying the fewest descriptors that can be used to yield the lowest CCS prediction error. The calculated descriptors for any candidate 2D structure arising from SIRIUS 4 can then be plugged into the model to yield a predicted CCS value.

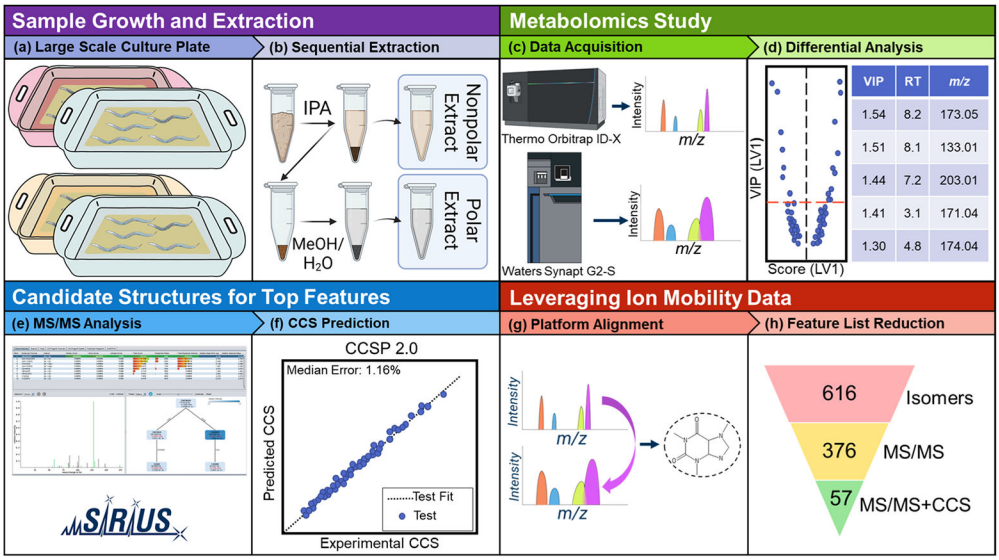

Figure 2.

Graphical overview of the metabolomics workflow employed in this study. *C. elegans* mutant strains were grown in tandem with growth-matched PD1074 reference strain samples (a). These cultures were harvested to aliquots of 200,000 worms, lyophilized, and then sequentially extracted, yielding nonpolar and polar fractions (b). All samples were analyzed on a Thermo Orbitrap ID-X platform. Pooled samples were reanalyzed on a Waters Synapt G2-S to provide complementary ion mobility data (c). Orbitrap data were used for differential analysis to select significant features of interest (d). Orbitrap MS/MS data were imported to SIRIUS 4[8] to generate candidate structures using CSI:FingerID[7] (e). The CCS value for each candidate structure produced by SIRIUS 4 was predicted using CCSP 2.0, an SVR-based machine learning algorithm trained with the McLean Unified CCS Compendium[11] data (f). Synapt ion mobility data were matched to Orbitrap data to provide experimental CCS values for differential features (g), which were then used to eliminate candidate structures falling outside the 3% error band (h).

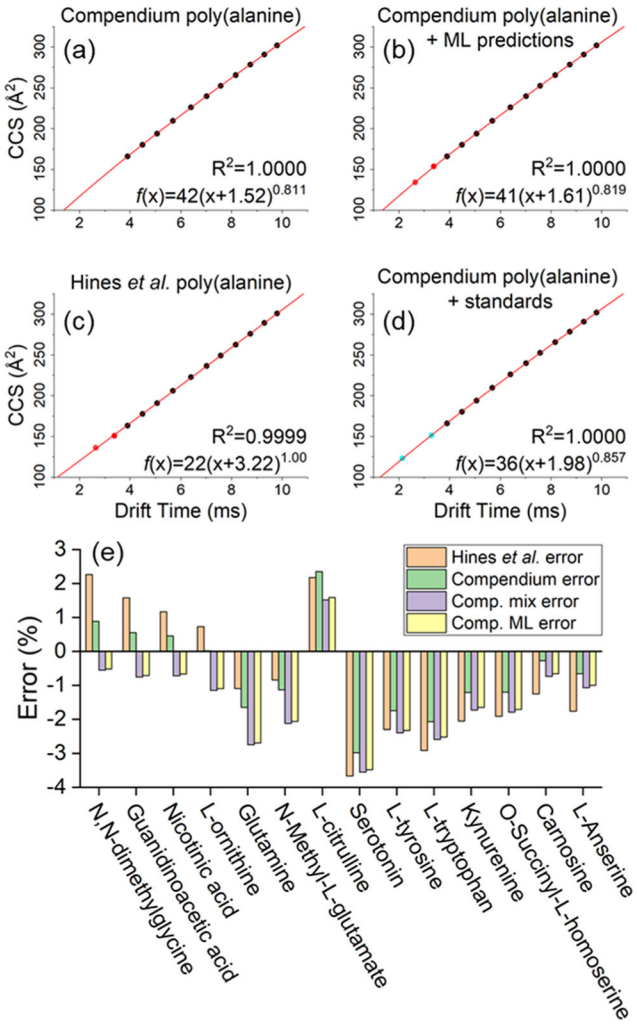

Figure 3.

Accuracy of four CCS calibration strategies was evaluated using a panel of 14 standards covering the 104–241 *m/z* range. Plot (a) shows a power law calibration curve using Unified CCS Compendium[11] data covering poly(alanine) oligomer lengths $n = 4–14$ (black points). To further extend the range of calibration, this series may be extended using ML predicted CCS values for poly(alanine) $n = 2–3$ (red points) as shown in plot (b) or by using poly(alanine) data from an alternate source (c). Alternatively, the poly(alanine) series may be supplemented with additional standards as in (d) where dimethylglycine and tryptophan (blue points) were used. CCS values for these 14 standards were calculated using each of the four power-law calibration curves, and then compared against Unified CCS Compendium[11] reported values for each standard. Errors for each calibration procedure are shown in (e).

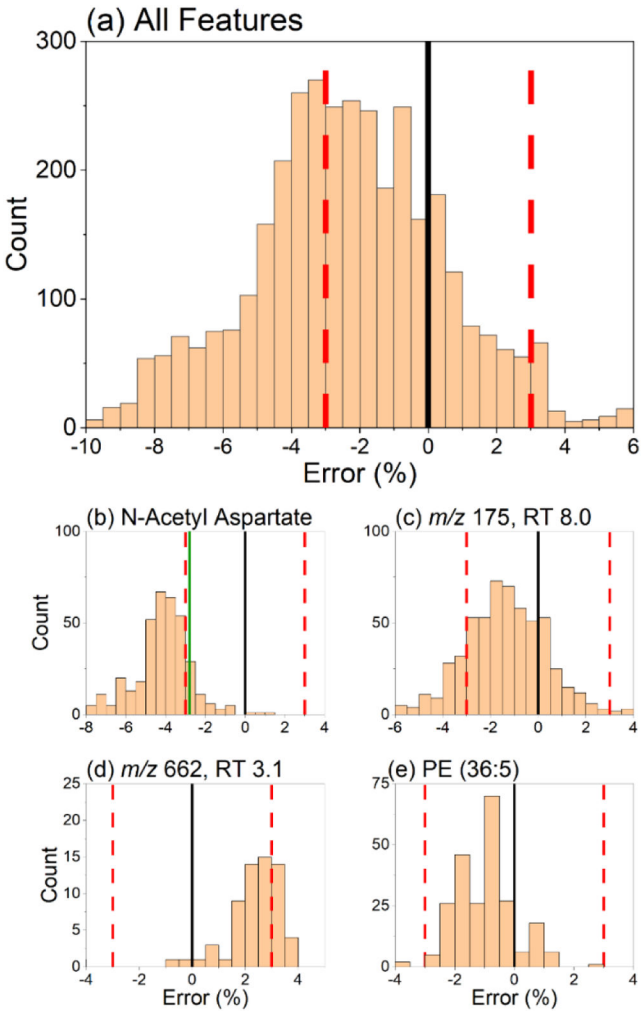

Figure 4.

Histogram describing the percent error between ML-predicted CCS values of SIRIUS 4 candidate structures ($n = 3495$) *vs* experimentally measured CCS. The error in these predictions was defined as in eq 1. Shown in (a) is the summation of errors for all the 19 differential features investigated, demonstrating an overall filtering success of 45.2% (1580 out of 3495). A negative bias toward lower-than-predicted experimental CCS values was observed. Individual errors for four features of interest are shown in plots (b–e). The solid black line represents the experimentally measured CCS value. The red dashed lines represent the ±3% CCS cutoff. The solid green line represents the error of the correct compound validated with a chemical standard.

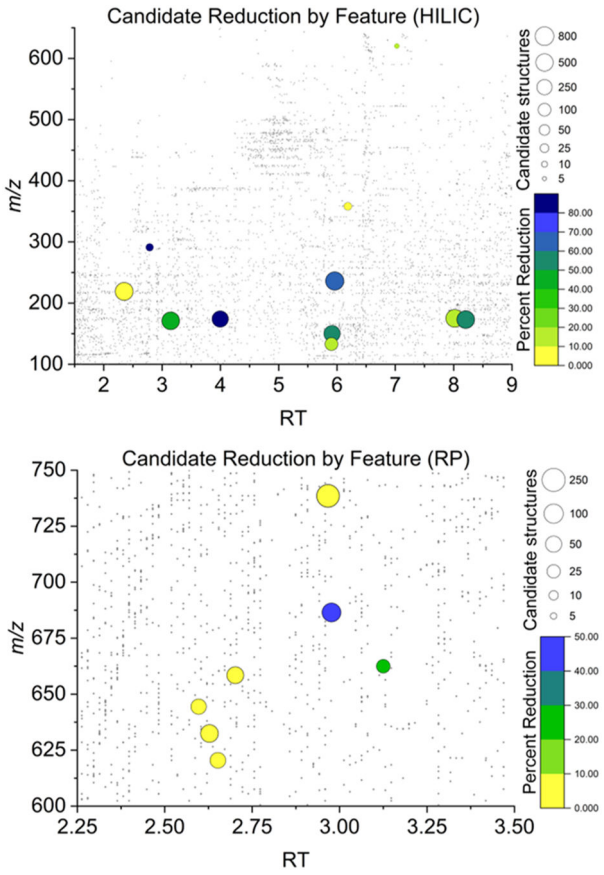

Figure 5.

Overall results from CCS-assisted annotation of unknown features. Each investigated feature is represented by a bubble with the size defined by the total number of MS^2-generated candidate structures and color defined by the percent of total candidates, which could be discarded by their CCS value. A background of gray dots represents all detected features.